Journal of Geophysical Research: Planets

RESEARCH ARTICLE
10.1029/2018JE005536

New Evidence of an Ancient Martian Ocean From the Global Distribution of Valley Networks

Ngai-Ham Chan[1,2], **J. Taylor Perron**[3], **Jerry X. Mitrovica**[4], **and Natalya A. Gomez**[1,2]

[1]McGill Space Institute, McGill University, Montréal, Québec, Canada, [2]Department of Earth and Planetary Sciences, McGill University, Montréal, Québec, Canada, [3]Department of Earth, Atmospheric and Planetary Sciences, Massachusetts Institute of Technology, Cambridge, MA, USA, [4]Department of Earth and Planetary Sciences, Harvard University, Cambridge, MA, USA

Abstract We examine the connection between true polar wander (TPW) and the evidence for an ancient ocean on Mars. Previous studies have investigated the plausibility of a Mars ocean by examining the topography of possible ancient sea level markers on the planet's surface. One such study argued that features interpreted as ancient shorelines display long-wavelength topographic variations consistent with postformational TPW (Perron et al., 2007, https://doi.org/10.1038/nature05873). In contrast, a second study argued that the elevations of possible ancient deltaic deposits associated with an ocean on early Mars are not consistent with the TPW scenario (di Achille & Hynek, 2010, https://doi.org/10.1038/ngeo891). Herein we revisit this issue by examining another marker of ancient shorelines—fluvial valley networks observed on the surface of Mars. Our results support the existence of an ancient Martian ocean and that long-wavelength deformation of related surface features (ancient shorelines and valley networks) was driven by some combination of TPW and surface loading associated with the formation of the Tharsis volcanic province.

Plain Language Summary Whether an ancient ocean existed on Mars has long been a controversial subject. On the one hand, past conditions predicted by climate simulations suggested that Mars might not have been able to sustain liquid water for long periods of time. On the other hand, there is an abundance of surface features such as shorelines, deltas, sediments, and valley networks that suggest widespread and persistent liquid water on Mars. While the features believed to trace out ancient shorelines do not lie on the same elevation today, they could have been shifted vertically by the movement of Mars' rotation pole (which caused a shift in the equatorial bulge) or by the formation of Tharsis—a cluster of large volcanoes. In this study, we present a new set of possible sea level markers: the valley networks that may have drained directly into an ancient northern ocean. We find that the elevations of these valley networks, along what would have been the shore of the northern ocean, are consistent with them being ancient sea level markers that had been subsequently shifted vertically by some combination of changes in Mars' rotation pole and the growing Tharsis volcanic bulge.

Key Points:
- Surface deformation due to true polar wander (TPW) in the Martian past caused sea level markers to deviate from a present-day equipotential
- Previous analyses of possible ancient sea level markers reached opposing conclusions on whether TPW is necessary to explain their topography
- Our analysis of the elevations of valley networks supports the TPW scenario and, by extension, the possible existence of an ancient ocean

Supporting Information:
- Data Set S1
- Data Set S2
- Supporting Information S1

Correspondence to:
N. H. Chan,
nhchan@me.com

Citation:
Chan, N.-H., Perron, J. T., Mitrovica, J. X., & Gomez, N. (2018). New evidence of an ancient Martian ocean from the global distribution of valley networks. *Journal of Geophysical Research: Planets*, *123*, 2138–2150. https://doi.org/10.1029/2018JE005536

Received 17 JAN 2018
Accepted 17 JUL 2018
Accepted article online 26 JUL 2018
Published online 27 AUG 2018

1. Introduction

The surface of Mars is marked by a variety of geologic and topographic features that suggest the past existence of a global hydrological system. These include contacts that resemble shorelines (Clifford & Parker, 2001; Parker et al., 1989, 1993), deltaic deposits (di Achille & Hynek, 2010; DiBiase et al., 2013, and references therein) sedimentary deposits (Lewis et al., 2008; Malin & Edgett, 2000), valley networks (Carr, 1995; Fassett & Head, 2008; Hynek et al., 2010; Matsubara et al., 2013), and other terrain forms (e.g., Moscardelli, 2014). Despite the abundance of such features, the existence of an ancient ocean, or even a sustained and/or widespread hydrological cycle, remains controversial (e.g., Ghatan & Zimbelman, 2006; Leverington, 2011). The controversy largely arises from the difficulty in reconciling the past conditions predicted by climate models and the conditions required to sustain water in liquid form for long periods of time (e.g., Fairén, 2010; Wordsworth et al., 2013, 2015; Wordsworth, 2016).

Several recent studies have used topography to investigate the Martian ocean hypothesis. Perron et al. (2007) showed that the long-wavelength topography of continuous contacts along the Martian surface is consistent with deformation of ancient shorelines caused by true polar wander (TPW) after the formation of the massive

Tharsis volcanic province. TPW is a secular reorientation of a planet's rotation axis with respect to its solid body driven by mass redistribution(s) on or inside a planet, such as mantle convection or changes in the location and thickness of glacial ice (Gold, 1955; Goldreich & Toomre, 1969). Perron et al. (2007) showed that the preferred TPW path satisfied a strong dynamic constraint that Tharsis remain on the planet's equator. In contrast, di Achille and Hynek (2010) analyzed the elevations of ancient deltaic deposits (manually selected to exclude isolated water bodies not connected to an ocean) and argued that they lie close to a present-day equipotential surface, concluding that these possible ancient sea level markers have undergone little postdepositional deflection by TPW or other processes. Concerning the deltaic deposits of di Achille and Hynek (2010), however, DiBiase et al. (2013) pointed out that the criteria used by di Achille and Hynek (2010) may have led to the inclusion of deltas that were deposited due to topographic changes rather than debouchment into a standing body of water. Most recently, Citron et al. (2018) have argued that the ancient shorelines formed before or at the same time as the emplacement of Tharsis and that the long-wavelength topography of the shorelines was driven by the loading and TPW associated with this emplacement.

In this article, we revisit the Martian ocean hypothesis by examining the topographic distribution of valley networks as a possible marker of an ancient equipotential. This is conceptually different from studies that use the geographical (lateral) distribution of surface features to calculate possible TPW (e.g., Bouley et al., 2016; Mutch & Saunders, 1976), in that we are using topographic (vertical) deflections to infer any TPW events. Valley networks are most abundant in the southern highlands where craters and regionally steep slopes, such as the dichotomy boundary and the walls of the Hellas impact basin, are common (Irwin et al., 2011). Valley networks were incised by shallow, channelized surface flows (Howard et al., 2005; Irwin et al., 2005, 2008) and could not have formed while an area was inundated by ocean water. Existing valley networks that were subsequently inundated by an ocean would likely have been obscured by erosion and sedimentation. The locations and elevations of downstream endpoints, or termini, of valley networks therefore constrain the maximum extent of a Martian ocean that existed at the time of, or subsequent to, valley network formation. Valley network termini (henceforth, VNT) near the dichotomy boundary, believed to be the approximate limit of the ancient ocean, are of particular interest. The locations and elevations of these VNT could form a set of shoreline markers, which could be consistent with either a present-day equipotential or an ancient equipotential that has since been deformed.

Based on an analysis comparing the valley network flow directions with topographic gradients, Phillips et al. (2001) concluded that the valley networks formed after a large fraction of the Tharsis rise was in place. In contrast, Bouley et al. (2016) reconstructed the pre-Tharsis figure of Mars and argued that the direction and location of the valley networks are consistent with this configuration; they thus concluded that the fluvial incision occurred during or before emplacement of Tharsis. Lacking widespread consensus on the timeline of these events, we will consider two scenarios for the deflection of VNT topography. The first, following Perron et al. (2007), assumes that the TPW event occurred after Tharsis had reached a location close to the equator. That is, we are testing the hypothesis that post-Tharsis TPW can reconcile the long-wavelength topography of the VNT. As noted by Perron et al. (2007), any such TPW path(s) would have been limited to the great circle $\sim 90°$ from the center of Tharsis, and any paleopole deduced from the present elevations of VNT would have to satisfy this strict dynamic constraint. We adopt a Monte Carlo approach to determine the paleopole that best fits the present-day topography of the VNT and its uncertainty. Second, following specific scenarios inferred by Citron et al. (2018), we consider cases in which Tharsis formation was concurrent with, or after, the ocean (see section 2.3 below).

In the next section, we describe the methodological and mathematical details of our analysis. Due to the relatively shallow slope of Arabia Terra, any inferences about shoreline processes in that region are potentially sensitive to small elevation changes caused by surface modification; we discuss this issue in section 3. The results are described in section 4, and discussed in section 5.

2. Methods and Data

Our goal is to test whether the elevation pattern of valley networks supports the hypotheses that (i) an ancient Martian ocean existed, and (ii) there exists discernible, long-wavelength deflection of the VNT that is consistent with an ancient equipotential surface. Such large-scale topographic deflections are expected if the planet's rotational bulge migrated due to a reorientation of its rotation axis (see section 2.2), and/or in

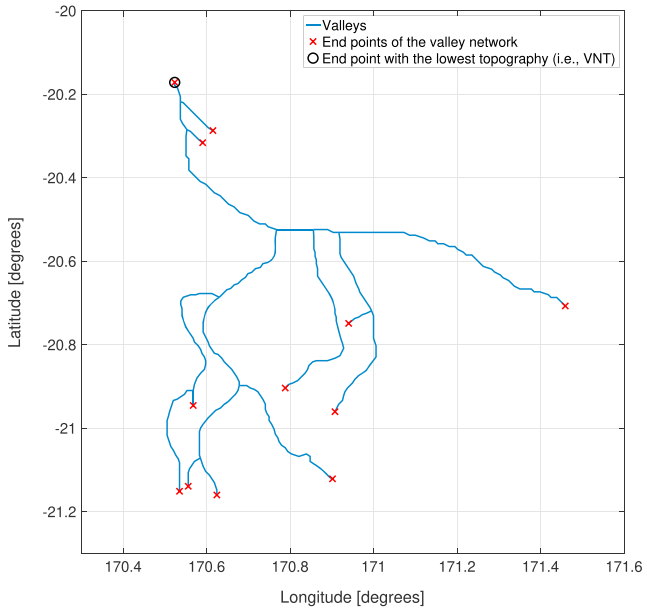

Figure 1. An example of a valley network showing its end points and the identification of the lowest end point (i.e., the valley network terminus, VNT).

response to the formation of Tharsis. Due to the antiquity of the valley networks, many processes, acting over a continuum of length scales, could have subsequently altered their elevations. However, in the present study we consider only long-wavelength deformation and do not consider any processes that may have given rise to localized, shorter-wavelength topographic variations in the valley networks.

2.1. Valley Network Termini as Paleoshoreline Markers

We use the global map of Martian valley networks produced by Hynek et al. (2010) in conjunction with a topographic map from the Mars Global Surveyor Mars Orbiter Laser Altimeter (MOLA) Mission Experiment Gridded Data Record (Smith et al., 2003), with a resolution of 128 pixels per degree, to find the terminus of each of the 9,879 mapped valley networks (Figure 1 provides an illustration of the identification of the terminus for a single valley network). Since the depth of an ocean could have varied through time, we need to limit our choice of valley networks by age. Studies have suggested that most of the Martian valley networks formed in the Noachian period (Carr, 1995; Fassett & Head, 2008; Hynek & Phillips, 2003; Hynek et al., 2010). Therefore, we initially included only the valley networks entirely contained within Noachian-aged terrains. However, when visually examining the data, we noted many areas where the pattern of flow displayed by the valley networks up to the Hesperian period are coherent with the earlier Noachian-aged valleys. This could mean that some valley networks had been incised on Noachian terrains during the Hesperian or that the evolution of many Noachian valley networks continued well into the Hesperian epoch. We thus loosen the age restriction in this analysis to include both Noachian- and Hesperian-aged valley networks. This age distinction is achieved by comparing the valley network coordinates against the geologic map of Mars (Tanaka et al., 2014). In order to limit uncertainties, only valley networks fully contained within a geological unit are assigned the age period of the unit. Figure 2a shows the Noachian and Hesperian VNT as dark blue and cyan points plotted on the Martian topographic map. We note that the age of terrains into which the valley networks incised represents only an upper limit for the age of the valley networks, since the valleys could have formed during any period subsequent to the formation of the terrain.

The next step is to identify all candidate VNT that would have drained directly into an ocean that covered the plains north of the dichotomy boundary (i.e., the topographic division between the southern highlands and the northern lowlands). By overlaying the MOLA topographic map with the age-separated valley networks (with their associated VNT marked), we visually examine all the valley networks along the entire length of the dichotomy boundary region. We separated the VNT into different categories based on criteria such as flow direction and geometry (both of the valley network and of its neighboring networks); number of tributaries; and proximity to valley networks on younger terrains. These categories are used to assess the (qualitative) likelihood of the selected VNT being at or near an ancient shoreline. For example, a tributary network that flows in a direction consistent with that of its regional neighbors is attributed higher confidence than a lone valley segment with similarly fragmented regional neighbors displaying highly variable flow patterns. In all cases, we seek the valley networks with termini that are closest to the northern plains compared to all the other valley networks in the immediate surrounding area (up to Hesperian in age). This process yielded 252 VNT (highlighted as cyan dots in Figure 2), 155 of which were attributed higher confidence than the rest (on the basis of directional coherence with regional neighbors and the presence of tributaries that clarify flow orientation); the group of 155 will form one of the groups in the Monte Carlo analysis described in section 2.3 below. Only the valley network map and the MOLA topography data were used in the process of manually selecting the VNT; this limits any potential bias in the selection procedure (e.g., from any visual connection to the Arabia or Deuteronilus contacts). We also left out the VNT around the Hellas impact basin because it is unclear whether or not it was inundated and, if so, what the water level was in relation to the northern ocean.

2.2. Accounting for Possible TPW

Following Perron et al. (2007), we account for the possibility that Mars may have undergone TPW subsequent to the disappearance of water from its surface. Using fluid Love number theory, we can calculate the topographic response to TPW. Given an ancient north pole at (colatitude θ', longitude ψ') in a coordinate system

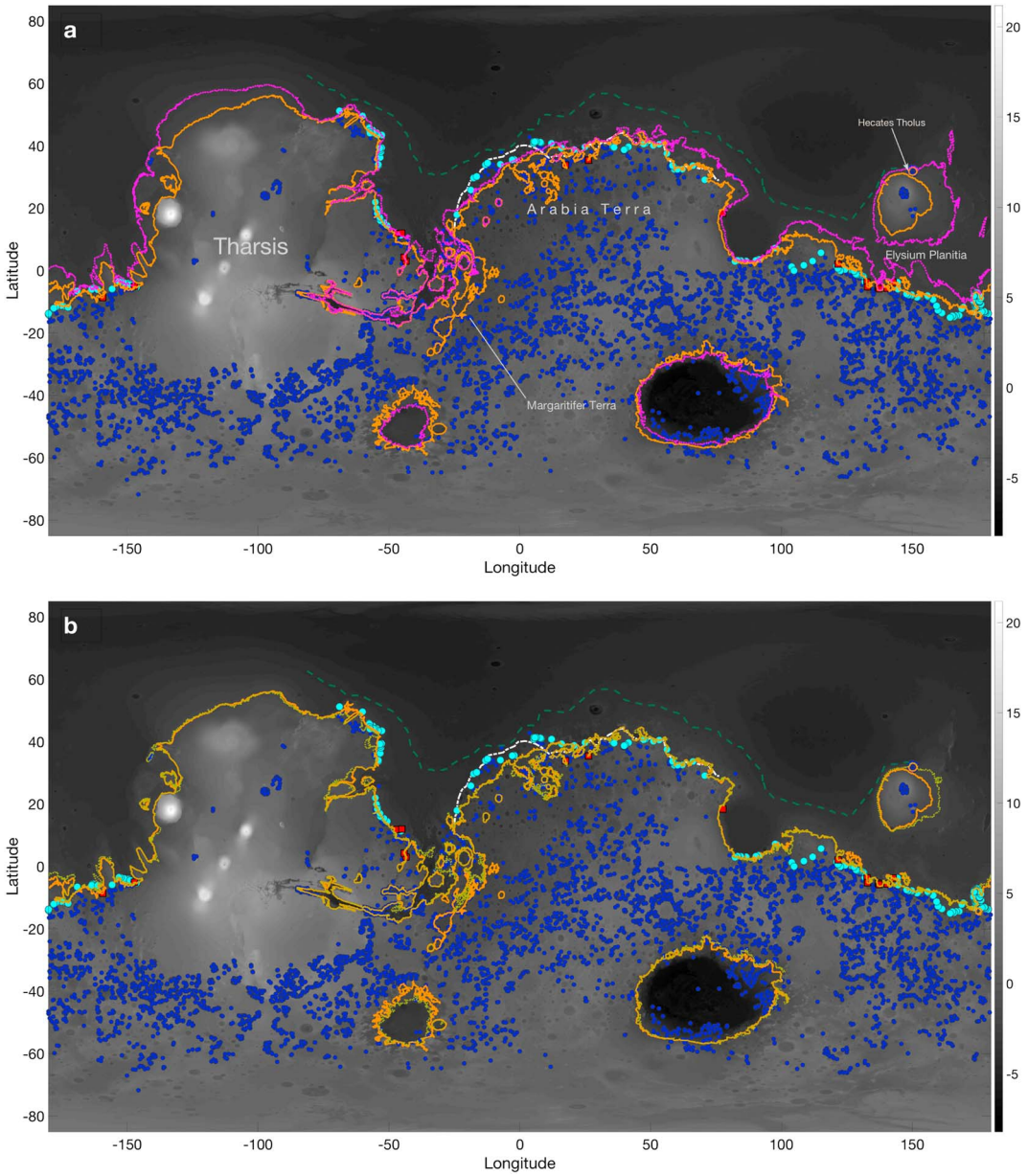

Figure 2. Topographic maps of Mars (the gray scale colors reflect present-day topography, in units of kilometers). The valley network termini (VNT) of the Noachian and Hesperian valley networks are shown as blue dots, with the manually selected near-shore VNT (see section 2.1) highlighted in cyan. The orange solid contours in both frames show the reconstructed shoreline of an ancient Martian ocean after the incorporation of true polar wander-driven topographic deformation (after the formation of Tharsis) associated with the paleopole location shown in Figure 4 (scenario P2007). (a) The magenta dotted contour shows the reconstructed shoreline inferred by di Achille and Hynek (2010) on the basis of delta elevations (a uniform shift of −2,540 m relative to the present-day equipotential, the areoid; scenario D2010). (b) The light green dotted contour shows the shoreline reconstructed on the basis of the analysis of Citron et al. (2018) in which topographic deformation is driven by the final (17%) stage of Tharsis emplacement (scenario C2018A; see main text). In this calculation, we adopt a *Z* shift that optimizes to fit the VNT, rather than the shift cited by Citron et al. (2018). To perform a fair comparison, the same topographic correction for erosional effects, based on the "bounded erosion: best fit" scenario of Evans et al. (2010), has been applied within Arabia Terra (see section 3) for all of the reconstructed shorelines. Craters and islands smaller than ~2° in diameter have been removed from all contours for clarity. Also plotted for reference are the (white dash-dotted line) Arabia shoreline and (green dashed line) Deuteronilus shoreline adopted by Perron et al. (2007) and Citron et al. (2018) in their analyses. The deltas included in the analysis of di Achille and Hynek (2010) are shown as red squares.

in which the present-day north pole is at ($\theta = 0, \psi = 0$), the centrifugal potential of this paleorotational state is given by (Lambeck, 1980)

$$\phi(\theta, \psi) = \frac{1}{3}\omega^2 a^2 - \frac{1}{3}\omega^2 a^2 P_{2,0}(\cos\gamma), \tag{1}$$

where ω is the rotation rate of the planet, a is its mean radius, and γ is the angular distance between (θ, ψ) and (θ', ψ'). The degree-2, order-0 Legendre polynomial is given by

$$P_{2,0}(\cos\eta) = \frac{1}{2}\left(3\cos^2\eta - 1\right), \tag{2}$$

where η is the angle between the position vector and the axis of symmetry. In our case, η will take on values of either angular distance γ or the colatitude θ. Since the expected variations in ω are small, we assume that it is constant. The difference between the paleocentrifugal potential and the present-day potential is then

$$\Lambda(\theta, \psi) = \frac{1}{3}\omega^2 a^2 \left[P_{2,0}(\cos\gamma) - P_{2,0}(\cos\theta)\right]. \tag{3}$$

The topographic response to a TPW event is then (Mound & Mitrovica, 1998)

$$\Delta T(\theta, \psi) = \frac{\Lambda(\theta, \psi)}{g}\left[h_f - \left(1 + k_f\right)\right] + Z, \tag{4}$$

where g is the gravitational acceleration at the surface, h_f and k_f are the degree-2 h and k fluid tidal Love numbers, and Z is a constant shift factor introduced to account for the fact that the equipotential defining the present-day areoid is not necessarily the same as the equipotential level at the ancient sea surface (Dahlen, 1976). This geographically variable change in topography occurs because a fluid surface (such as sea level) and the planet's solid surface respond differently to the load $\Lambda(\theta, \psi)$. An illustration of the geometry of ΔT is shown in Figure S1 in the supporting information. Using equations (3) and (4), we can correct the present-day topography for the deformation that would have been caused by the planet shifting from its ancient orientation of rotation to its present orientation.

2.3. Testing TPW Scenarios

As noted above, we test a scenario (henceforth scenario P2007) consistent with the assumption of Perron et al. (2007) in which TPW that drove the observed long-wavelength deformation of both the Arabia and Deuteronilus shorelines occurred after the ocean disappeared and Tharsis was fully emplaced. Specifically, we seek to find a paleopole that yields minimum differences between ΔT and the present-day topography of the VNT. In the associated calculations, we adopt values of h_f and k_f (in equation (4)) consistent with a Mars model (based on the *M13* model of Zharkov and Gudkova, 2005) having an elastic lithosphere that is 200 km thick, resulting in the Love numbers $h_f = 1.656$ and $k_f = 0.899$. We chose this elastic thickness to facilitate comparisons with the results from Perron et al. (2007). Results from Mars models with elastic thicknesses of 15, 48, and 110 km are included in the supporting information (also see discussion on elastic thicknesses in section 3).

In the search for the best fit pole we used a spatial resolution of 1° for the geographical coordinates (latitude and longitude), and 50 m for constant shift Z in equation (4). For each possible paleopole location, we computed the Z that minimizes the least squares misfit between the present-day VNT elevations and ΔT. We then took the pole location that minimizes the overall misfit to be the best fit paleopole. Furthermore, to check for the effect of outliers, we also assessed the fit using a maximum-likelihood method based on an L1 norm (Aster et al., 2005§ 2.4). The two approaches resulted in essentially identical best fit paleopoles. For this reason, we adopt the least squares approach in the remainder of this article.

In order to estimate the statistical uncertainty of our results in the absence of a priori knowledge of the data errors, we employ a Monte Carlo algorithm to construct an ensemble of resampled data sets, with the size of each instance being equal to the original, by randomly picking from the original data set (i.e., the 252 VNT shoreline markers discussed above). A random number generator with uniform distribution is used for each instance of the resampled data sets. In the terminology of statistics, this process is called *bootstrapping with replacement* or *case resampling with replacement* (e.g., Chernick et al., 2011; Efron, 1979). Furthermore, the resampling is *stratified*. That is, for each instance, the resampling is performed separately on the group of 155 VNT ascribed higher confidence (see section 2.1) and the remaining 97 VNT. This ensures that the resampled

data will carry through the qualitative assessments made during the VNT selection process, by maintaining the same proportion of confident and less confident data in each of the resampled data sets. For each resampled data set constructed, we compute a misfit for every possible paleopole location as described in section 2.2. In total, 40,000 iterations were performed. If our data set of VNT were truly random (i.e., they show no resemblance to any possible equipotential markers), the results from such a Monte Carlo process would yield no clear tendencies for the location of the best fit paleopole. On the other hand, if our data represent markers of a past equipotential, we would obtain a (quantitative) likelihood of the paleopole being at some specific location.

In addition to the above test, we consider two scenarios inferred by Citron et al. (2018), who argued that Tharsis formed at the same time as, or after, the ocean. The Citron et al. (2018) study, like Perron et al. (2007), was based on fitting the long-wavelength topography of the Arabia and Deuteronilus shorelines. In the timeline they presented, ocean drying from the older Arabia shoreline to the younger Deuteronilus shoreline took place during the first 83% of Tharsis formation and was accompanied by a ~20° TPW event that brought Tharsis to its current equatorial position. Vertical deflection of the Arabia shoreline was, according to them, driven by the total emplacement of Tharsis and the ~20° TPW event, while the deflection of the Deuteronilus shoreline was driven by the final 17% emplacement of Tharsis. In the first scenario (henceforth C2018A), we assume that the topography of the selected VNT was deflected in the same manner as the Deuteronilus shoreline in Citron et al. (2018), that is, by the final 17% of Tharsis emplacement. In a second scenario (henceforth C2018B), we assume that the topography of the VNT were deflected in the same manner as the Arabia shoreline in Citron et al. (2018); that is, Tharsis formed, and the ~20° TPW took place, entirely after the selected VNT were incised. In both scenarios, we do not adopt the constant shift Z (in equation (4)) cited by Citron et al. (2018), but rather we treat Z as a free parameter and vary it to provide the best fit to the present-day topography of the VNT. We correct for the crustal deformation due to the Tharsis load using displacement fields provided by the authors, and we compute the deformation driven by the ~20° TPW using equation (4) and the Mars model with the same lithospheric thickness adopted by Citron et al. (2018) (58 km).

As a final case, we consider the scenario preferred by di Achille and Hynek (2010), who argued that the elevation of deltas near the dichotomy boundary was best fit by a shoreline that followed the present-day areoid of Mars with the exception of a constant height shift Z (henceforth scenario D2010).

3. Surface Modification in Arabia Terra

As a consequence of the relatively shallow slope of Arabia Terra (the area bound approximately by 20°W to 20°E and 0°N to 35°N, south of the dichotomy boundary), small elevation changes in the region would have corresponded to large differences in the geographic locations of equipotential features such as shorelines. Therefore, the neglect of surface-modification processes such as erosion may impact our inferences of TPW if VNT from the region are included in the analysis. Evans et al. (2010, and references therein) cited geophysical and morphological evidence suggesting that Arabia Terra had experienced a major phase of erosion. Using the Mars Global Surveyer MOLA altimetry data and the gravity data from the Mars Reconnaissance Orbiter, they calculated erosional loads as well as the corresponding crustal flexure for seven model erosional scenarios.

In the results based on scenario P2007 discussed below, we consider two erosional models presented in Evans et al. (2010): the "bounded erosion: best fit" and "uniform erosion: best fit" scenarios. These two "best fit" scenarios were determined by minimizing the gravity anomaly differences between the interior and exterior of Arabia Terra across both the northern (lowland) and southern (highland) boundaries (Evans et al., 2010). The other five scenarios are identified by Evans et al. (2010) as either limiting cases or (in one case) incompatible with other observational constraints. In each of the two cases we chose to adopt from Evans et al. (2010), we use the combined elevation change resulting from both erosion and the associated crustal flexural response to correct the present-day topography. For the case of post-Tharsis TPW, this *corrected* topography is then used in conjunction with equation (4) to calculate the best fit location of the paleopole. It is interesting to note that four of the remaining five erosion scenarios (all but the "flexural fit" scenario) derived by Evans et al. (2010) yield shoreline reconstructions in our analysis (i.e., reconstructions that include a correction for post-Tharsis TPW) that put large swaths of VNT-containing Arabia Terra under water.

The flexural responses to the erosional loads presented in Evans et al. (2010) were calculated in that study using a uniform lithospheric plate with an elastic thickness of 15 km, whereas we use a 200-km elastic

lithosphere in equation (4) above. We do not consider this to be a contradiction because the timing of the erosional modification to Arabia Terra was much earlier in the P2007 scenario than the TPW event that deformed the original elevation of the VNT connected to sea level. Evans et al. (2010) noted that erosion (or other surface modification processes) in Arabia Terra likely took place prior to the Hesperian epoch. As we discussed in section 2.1, a significant number of the VNT in our database are found on Hesperian terrains, and our P2007 analysis assumes that the episode of TPW event occurred after their emplacement. The elastic thickness of the Martian lithosphere would have increased over time as the planet cooled, with estimates ranging from below ~20 km in the Noachian epoch to ~300 km at present day (Grott et al., 2013; Phillips et al., 2008). In any case, our analysis shows that the location of the best fit paleopole is only weakly dependent on the thickness of the elastic lithosphere adopted in the TPW calculation (see Figure S2 in the supporting information; for these results, the elastic lithospheric thickness adopted in the flexural calculation associated with the Arabia Terra erosional response was fixed to 15 km).

For a consistent comparison of the scenarios, in the results shown below a correction to the topography based on the "bounded erosion: best fit" scenario of Evans et al. (2010) is also applied within Arabia Terra for the reconstructed shorelines based on the scenarios C2018A, C2018B, and D2010. Evans et al. (2010) pointed out that the erosion in Arabia Terra may have occurred over time (instead of being a single event), noting that the erosional load corresponding to a 15 km elastic thickness of the lithosphere likely represents an upper limit (since the lithosphere was expected to thicken over time). This is because Evans et al. (2010) determined the erosional load by fitting the effects against the relative gravity anomaly across the boundaries of Arabia Terra for a specified lithospheric thickness; a thicker lithosphere would result in lower estimates of the erosional load. Due to uncertainties in the duration of the erosion in Arabia Terra and in its timing relative to the various stages of Tharsis formation, our correction for erosion in the scenarios of Citron et al. (2018; C2018A and C2018B), who used an elastic lithospheric thickness of 58 km, also likely represents the upper limit.

Aside from erosion, it has also been suggested that a volcanic province existed in Arabia Terra near the dichotomy boundary (Michalski & Bleacher, 2013), which roughly coincides with the region covered by the erosional scenarios discussed above. Clearly, a deeper understanding of the area's geological history would help discern what combination of processes may have altered the region's topography and morphology during and subsequent to the formation of the valley networks.

4. Results

We begin by considering scenario P2007. Figure 3 shows the probability densities of the three parameters that were varied in the Monte Carlo analysis: the latitude and longitude of the paleopole and the potential (constant) offset in the areoid, Z. The median values of the latitude and longitude of the paleopole and the areoid shift are 75°N, 33°W, and −1,550 m, respectively. The 95% confidence bounds of the Z parameter are ±150 m. The non-Gaussian nature of the latitude and longitude probability distributions results in uncertainties that are less straightforward to characterize. The 2.5th and 97.5th percentiles are, respectively, 71°N and 78°N for the latitude and 75°W and 7°W for the longitude. Using these percentile values as guides, the location uncertainty of the paleopole roughly conforms to within ~10° of arc from the median position. The location of the median paleopole is shown in Figure 4, labeled V. The results in Figure 3 adopt the "bounded erosion: best fit" scenario of Evans et al. (2010) to correct the topography of Arabia Terra for erosional effects.

Figure 2a shows the reconstructed location of the paleoshoreline (orange contour) we infer from the aforementioned median values. That is, the shoreline corresponds to the median Z level of −1,550 m after the correction of present-day topography for the TPW implied by the paleopole labeled V in Figure 4, and the correction of Arabia Terra topography for erosional effects. The same figure shows the paleoshoreline (magenta dotted contour) inferred by di Achille and Hynek (2010) on the basis of their analysis of deltaic deposits but corrected for the same erosional effects in Arabia Terra.

Figure 2b is identical to Figure 2a except that the light green dotted contour shows the paleoshoreline inferred by adopting the C2018A scenario of Citron et al. (2018), that is, by correcting present-day topography for the deformational and gravitational impact of the final 17% of Tharsis emplacement (see Matsumaya & Manga, 2010). As we have noted, this partially formed Tharsis topography model was shown by Citron et al. (2018) to be consistent with the Deuteronilus shoreline. The equipotential shift, Z, in this case is −1,650 m, which provides an optimal fit to the topography of the VNT (instead of the $Z = -3{,}680$ m used to fit the Deuteronilus

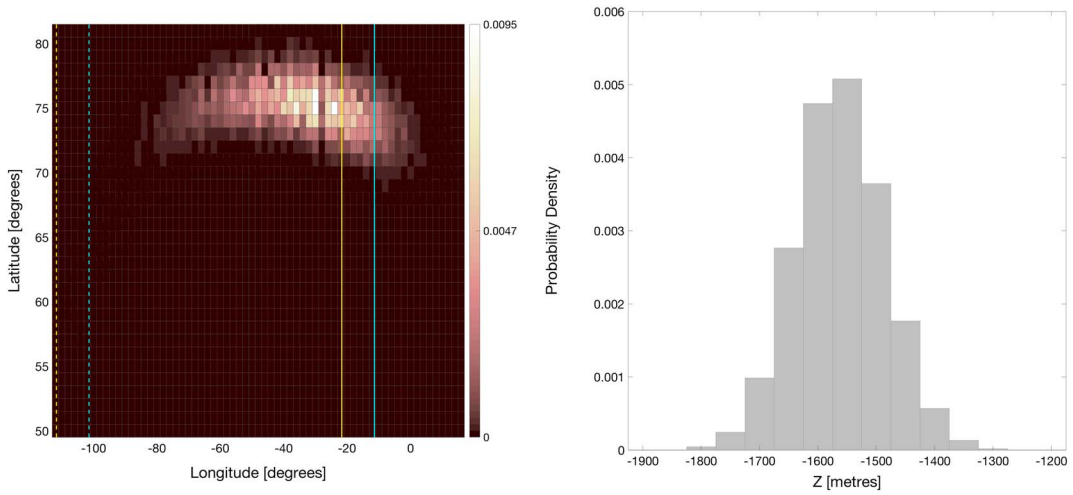

Figure 3. Probability densities of (left) the geographical location of the paleo-north pole, and (right) the uniform shift in the areoid, *Z*, derived from the Monte Carlo analysis of scenario P2007. The median values for these quantities are 75°N for the latitude, 33°W for the longitude, and −1,550 m for *Z*. The 2.5th and 97.5th percentiles are 71°N and 78°N for the latitude, 75°W and 7°W for the longitude, and −1,400 and −1,700 m for *Z*, respectively. See section 4 for more details on the uncertainties. (Note that the best fit paleopole was determined from the aggregate results of the Monte Carlo process and not the 2-D probability distribution as shown, thus avoiding any potential geometric biases.) The solid vertical lines on the left pane are the locations of the great circles 90° away from the center of Tharsis as estimated by (yellow) Zuber and Smith (1997) and (cyan) (Matsuyama & Manga, 2010). The great circles passing through the center of Tharsis are also shown as dashed vertical lines, with the same color scheme. See section 5 for details.

shoreline in Citron et al. (2018)). Figure S3 shows the analogous results for the scenario C2018B, in which the present-day topography is corrected for the full effects of Tharsis emplacement and the associated ~20° of TPW.

There are important residual differences in the paleo, predeformation topography between the case in which an ancient equipotential surface corresponding to the VNT was deformed by post-Tharsis TPW (scenario P2007) and the case in which such equipotential was deformed by late-stage Tharsis formation (scenario C2018A), that is, between the two cases corresponding to the shoreline inferences in Figure 2b. These differences resemble a degree 2, order 1 spherical-harmonic pattern (Figure S4).

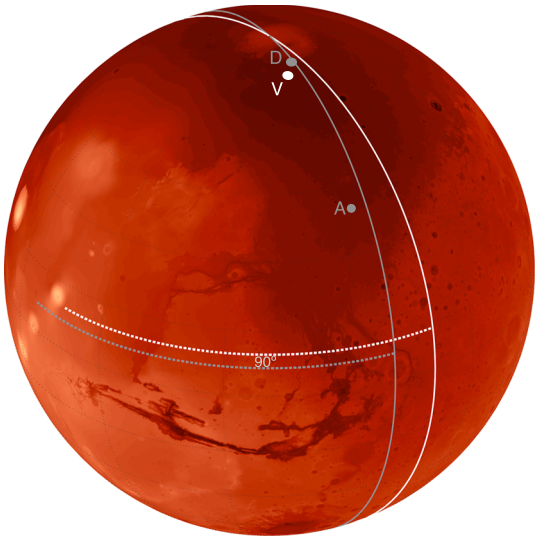

Figure 4. Map of Mars centered around the midlatitude region west of Arabia Terra. The white dot (labeled V) denotes the location of the median paleopole inferred in scenario P2007 of this study. The paleopoles inferred by Perron et al. (2007) on the basis of the Arabia and Deuteronilus shorelines are shown in gray, and labeled A and D, respectively. The great circle 90° away from the center of Tharsis (9.8°N, 258.6°E; see Matsuyama & Manga, 2010) is also shown in white; the gray line is the equivalent but based on a location for the center of Tharsis estimated by Zuber and Smith (1997).

As a relative measure of the fit, we also calculated the closest great-circle distances between each of the near-shore VNT (cyan dots in Figure 2) and each of the inferred paleoshorelines (taken to be the longest, continuous part of the contours, such that islands and craters are excluded). The resulting mean values of these distances (henceforth mean distances) are 52 km for the shoreline corresponding to scenario P2007 (Figure 2, orange contour), 149 km for the shoreline inferred by di Achille and Hynek (2010) (Figure 2a, magenta dotted contour), and 54 and 253 km for the shorelines inferred by adopting scenarios C2018A and C2018B of Citron et al. (2018), respectively (Figure 2b, light green dotted contour; Figure S3, light green dotted contour). When the erosion corrections are excluded from the scenarios of Citron et al. (2018), the mean distance becomes 67 km for C2018A and remains 253 km for C2018B.

Using the "uniform erosion: best fit" case of Evans et al. (2010) as the initial correction of Arabia Terra topography in scenario P2007, the predicted location of the paleopole and uniform shift of the areoid is 75°N, 25°W, −1,550 m. The resulting shoreline reconstruction is shown in Figure S5 (the color scheme and labeling of which are analogous to Figure 2). The mean distance between the VNT and the shoreline inferred in this case is 61 km, whereas the mean distance to the shoreline inferred by di Achille

& Hynek (2010; corrected for erosion) is 153 km. The mean distance for the C2018A and C2018B (Citron et al., 2018) shoreline reconstructions (corrected for erosion and optimized equipotential level) are 64 and 250 km, respectively.

5. Discussion

The probability distributions shown in Figure 3, which represent a test of scenario P2007, display a preferred paleopole location. This clustering suggests that the distribution of the VNT is not random (as discussed in section 2.3). Furthermore, as discussed in section 1, the path of any TPW subsequent to the formation of the Tharsis volcanic province is unlikely to have diverged significantly from the great circle ~ 90° away from the center of Tharsis. Two great circles, based on two different estimates of the centroid of Tharsis (Matsuyama & Manga, 2010; Zuber & Smith, 1997), are superimposed on Figure 4. (Their corresponding longitudes are also marked in the left pane of Figure 3.) In the context of Figure 3 (left pane), 86% of the results from our Monte Carlo analysis lie within 30° of either of the great circles 90° away from Tharsis, while only 2.9% lie within 30° of the great circles passing through either centroids of Tharsis. We conclude that our inference of the paleopole location is consistent with this relatively stringent dynamical constraint.

Our inferred mean paleopole location for scenario P2007 is ~35° along a great circle from the location inferred by Perron et al. (2007) on the basis of the present-day long-wavelength topography of the Arabia shoreline (labeled A in Figure 4), and ~ 5° from the location they estimated on the basis of the topography of the Deuteronilus contact (labeled D in Figure 4). The small TPW is more consistent with the conclusion of Daradich et al. (2008) that large (on the order of 90°) TPW is unlikely even along the great circle 90° away from the center of Tharsis. The Arabia contact is older than the Deuteronilus contact (Clifford & Parker, 2001), and there is morphological evidence that the latter formed during the Late Hesperian or even Early Amazonian period (Erkeling et al., 2012). However, the age of the VNT relative to these topographic features is uncertain. Assuming a unidirectional TPW path, the results summarized in Figures 3 and 4 suggest that the age of the VNT is intermediate to the ages of the Deuteronilus and Arabia contacts. This is consistent with the inclusion of Hesperian-aged networks in our analysis. Assuming a drying trend in the Martian ocean, the mean present-day elevation of these features provides a somewhat coarse test of relative age. The mean elevation of the VNT is −1.77 km, whereas the Arabia and Deuteronilus shorelines have mean elevations of −1.68 km and −3.76 km, respectively (Clifford & Parker, 2001). This is again suggestive of VNT ages that are intermediate to the ages of the Arabia and Deuteronilus contacts. However, while the VNT are closer in mean elevation (and geographically) to the Arabia shoreline, the results in Figure 4 suggest that they are closer in age to the Deuteronilus contact, further highlighting the uncertainty in the relative ages of the two contacts.

We note that the VNT we have selected as the most robust extend over ~ 280° of longitude, a much greater distance than the dimensions of Arabia or Deuteronilus shorelines analyzed by Perron et al. (2007; see Figure 2). In this regard, the inference of the paleopole location associated with the VNT may be more robust than those based on the shorelines.

The discrepancy between the reconstructed shorelines shown in Figure 2a is due to a combination of the TPW-induced perturbation in topography we have applied and the ~ 1 km difference in Z cited by di Achille and Hynek (2010) relative to our estimate. As indicated by the mean distances between each of these shorelines and the VNT, our shoreline reconstruction provides a substantially improved fit to the location of the VNT. This is most noticeable in both northeast Arabia Terra to the northwest of Isidis Planitia (a region extending from roughly 25°N to 40°N and 55°E to 75°E) and along Elysium Planitia (roughly, 10°S to 10°N and 120°E to 170°E). In both regions, the area between the two shoreline reconstructions is nearly devoid of valley networks of any age. Thus, if the ancient shoreline coincided with the inference of di Achille and Hynek (2010), then it would mean that there was either an abrupt and coherent termination of valley incision a few hundred kilometers onshore, or a complete erasure of all valleys in a region extending from the VNT to that reconstructed shoreline, across a region that extends laterally over thousands of kilometers. The latter scenario is unlikely, but the former may be possible if the local topographic gradient across the entire region decreases abruptly. We note that, for ~ 100 km beyond the final reaches of valleys toward the northern plains, the topographic gradients are comparable to those directly southward (on the highland side, where VNT exist), before ultimately transitioning into the flat, smooth topography characteristic of the northern plains. Based on these similar slopes, some valley incision should have occurred in the area downslope (i.e., northward) if this area were above sea level, as the di Achille and Hynek (2010) shoreline implies; yet no evidence of incision

is visible. We conclude that the di Achille and Hynek (2010) reconstruction of paleo-sea level is inconsistent with the location of the VNT.

Moreover, the shoreline inferred in our main result is also more consistent with the locations of the deltas included in the analysis of di Achille & Hynek (2010; shown as red squares in Figure 2) than the present-day equipotential inferred in their study. Indeed, the mean distance between the deltas and our shoreline is 25 km, compared to 118 km between the deltas and the reconstructed shoreline of di Achille and Hynek (2010).

Citron et al. (2018) suggested that the formation of Tharsis and its associated TPW caused topographic deflections that could account for the long-wavelength topography of the Arabia and Deuteronilus shorelines, without the need to invoke any additional TPW. Could Tharsis formation alone account for the long-wavelength topography of our VNT as well? Figure 2b shows the shoreline inferred from the topography of Citron et al. (2018) with a partially formed Tharsis (light green dotted contour; i.e., scenario C2018A), with Z shifted to best fit the VNT and with the erosion correction of the Arabia Terra topography applied. The mean distance between that inferred shoreline and the VNT is 54 km, compared to 52 km in the case of the shoreline inferred in our result for scenario P2007. (These mean distances are 25 km and 29 km, respectively, if we consider the deltaic deposits of di Achille & Hynek, 2010, instead of the VNT.) We conclude that the topography associated with the scenario C2018A is also consistent with the long-wavelength topography of the VNT. (Considering that the correction for erosion in Arabia Terra is likely an upper limit, as discussed in section 3, this C2018A result represents the best case scenario in terms of the fit between the inferred shoreline and the VNT. If we reduced the erosion correction toward 0, the affected segment of the inferred shoreline would move toward the interior of Arabia Terra, increasing the mean distance between shoreline and VNT to 67 km.)

Despite the similarities in the inferred shorelines, there are differences between predeformation topographies suggested by scenarios C2018A and P2007 (i.e., between the cases corresponding to the two shoreline inferences in Figure 2b; see Figure S4). The VNT all fall along regions where the difference in topography is small, which explains why the inferred shorelines are so similar. However, the topographies do differ in Margaritifer Terra, where there are valley networks (not included in our analysis) that coincide with the shoreline inferred in scenario P2007 (i.e., the post-Tharsis TPW case). Future data or analyses on the ages of the valley networks in the region may provide enough information to distinguish between these two deformation scenarios.

There is a large difference between the Deuteronilus shoreline and the VNT, both geographically (evident in the gap between the green dashed line and the contours in Figure 2b) and in the mean elevations (−3.76 km vs. −1.55 km). This is in contrast to the geographical (and mean-elevational) proximity of the inferred shorelines in Figure 2b (both cases) to the older Arabia shoreline. Aside from the aforementioned uncertainty in the relative ages of these features, this also highlights the uncertainty of the distances between the VNT and the actual paleoshore. This gap could arise due to erasure of the lower valley networks due to erosion, sediment aggradation (or lack of incision) on surfaces with gentle topographic gradients, or some combination of both. Concerning the second possibility, we note that the Deuteronilus shoreline is situated on the smooth lowlands in the Northern Hemisphere.

We have also tested the pre-Tharsis topography (i.e., completely removing Tharsis and the ~20° of TPW it had driven) that Citron et al. (2018) showed to be consistent with the Arabia shoreline, that is, scenario C2018B. The inferred shoreline in that case fit far worse than any other cases discussed in this article, with a mean-distance of 253 km between the inferred shoreline and the VNT (Figure S3).

Using the "uniform erosion: best fit" model from Evans et al. (2010) instead of the "bounded erosion" model, we found that the resulting paleopole is identical to the median paleopole inferred when testing the P2007 scenario except for the longitude prediction. Nevertheless, the longitude value in this case (25°W) remains well within 1 quartile of the median longitude in Figure 3. Comparing the two erosional models by Evans et al. (2010) in Arabia Terra, the shoreline inferred in Figure S5 ("uniform erosion: best fit") bends noticeably further inland over Arabia Terra than the result in Figure 2a ("bounded erosion: best fit"). Considering the larger number of valley networks (including those not used in our paleopole fits) that are submerged in Figure S5, and the larger mean distance for this case (61 vs. 52 km for the P2007 scenario, and 64 vs. 54 km for the C2018A scenario), we conclude that the "bounded erosion: best fit" scenario used in Figure 2a is preferred.

Finally, we note a geographical consistency between the locations of VNT and our reconstructed shoreline for scenario P2007 around Hecates Tholus volcano (northeast of Elysium Mons) and in Margaritifer Terra (east southeast of Valles Marineris), even though these VNT were not included in the Monte Carlo analyses

discussed above (Figures 2a and 2b). In contrast, a significant cluster of VNT remain submerged in northwestern Arabia Terra in all cases, regardless of whether or not TPW is invoked as a mechanism for perturbing topography. This reinforces our earlier suggestion, that a deeper understanding of the geological history of Arabia Terra—a region with relatively shallow slope—will be important for any future effort to constrain global scale processes that have perturbed the elevation of surface features associated with ancient Martian sea levels.

6. Conclusions

We analyzed the elevations of Noachian and Hesperian valley networks near the dichotomy boundary, believed to be the approximate limit of a northern ocean, and found that they are consistent with an equipotential surface that was subsequently deformed by a TPW event (i.e., scenario P2007). In this analysis, we took into account the effect of erosion in Arabia Terra (Evans et al., 2010) due to its relatively shallow slope, which causes inferred shoreline positions to be particularly sensitive to small elevation changes in that region. By removing the erosional effect on the elevations of the VNT, we determined that the median best fit paleopole of Mars when the valley networks would have been draining into an ocean is at 75°N, 33°W, with a sea surface height at −1,550 m. The uncertainty range of the estimated paleopole location is approximately 10° of arc from the median position, and the uncertainty of the sea surface height inference is ±150 m. Although this result is based on a Martian planetary model with an elastic lithospheric thickness of 200 km, we found that the location of the best fit paleopole is only weakly dependent on the thickness of the elastic lithosphere (see supporting information). Through a Monte Carlo estimation of uncertainties, we conclude that our result is not due to random chance. Moreover, within uncertainty, the location of our inferred paleopole falls along the same great circle as those inferred by Perron et al. (2007) and, likewise, satisfies the strong dynamical constraint that the TPW path should keep the Tharsis volcanic province on the equator.

We have also found that the topographic deformation driven by the last 17% of Tharsis emplacement, shown by Citron et al. (2018) to be consistent with the long-wavelength deflection of the Deuteronilus shoreline (i.e., scenario C2018A), is also consistent with the long-wavelength topography of the VNT (Figure 2b, light green dotted contour), after the correction for erosion in Arabia Terra and an equipotential shift to best fit the VNT. This raised the question of how close the VNT would have been to the paleoshore. Furthermore, in light of the relative age uncertainties between the Arabia shoreline, Deuteronilus shoreline, the valley networks, and Tharsis, the relative timing (or relation) between the P2007 and C2018A scenarios for long-wavelength deformation of the Martian crust is difficult to determine without additional information. A particular area of interest is in Margaritifer Terra, where the shoreline inferences of these two cases differ; analyses on the relative ages of the valley networks in that region could help distinguish between the two cases shown in Figure 2b.

In contrast to this ambiguity, we conclude that scenario C2018B (adopted from the case in Citron et al., 2018, that best fits the Arabia shoreline), in which it is assumed that Tharsis formed, and the ~20° TPW took place, entirely after the deposition of the shoreline markers is inconsistent with the long-wavelength topography of the VNT (Figure S3). We arrive at a similar conclusion for the scenario of di Achille and Hynek (2010), defined by a uniform shift of the present-day equipotential (Figure 2a, magenta dotted contour). The reconstructed shorelines associated with scenarios P2007 and C2018A trace the location of the VNT better, while scenario D2010 leaves extensive areas *on-shore* without evidence of valley incision. The local topographic gradients in these areas are similar to those in regions where valley networks exist, suggesting that the lack of incision in these areas is not simply a consequence of gentle slopes.

The shoreline inferred in scenario P2007 (Figure 2, orange contour) is consistent with the locations of valley networks around Hecates Tholus volcano and in Margaritifer Terra despite their not being included in the inference procedure. Moreover, the shorelines associated with scenarios P2007 and C2018A are geographically more consistent with the deltas included in the analysis of di Achille & Hynek (2010; shown as red squares in Figure 2) than the equipotential surface they inferred. We conclude that our results provide further support for the existence of an ancient ocean, the shoreline markers of which were substantially deflected after the ocean disappeared.

Acknowledgments
We thank James Tuttle Keane and an anonymous reviewer for their helpful suggestions. We are grateful to Alexander Evans for providing data describing the inferred erosion of Arabia Terra. We also thank Brian Hynek for making the valley network data available, Rossman Irwin for discussions about valley networks, and Isamu Matsuyama for discussions about true polar wander. The coordinates and elevations of the selected subset of valley network termini (described in section 2.1) are available as supporting information in the format of tab-delimited text files; the two files correspond to the two stratified resampling groups (described in both sections 2.1 and 2.3). All the other data used in this article are available via the respective references cited. N. H. C. is supported by the McGill Space Institute and National Science and Engineering Research Council (NSERC). J.T.P. thanks Harvard University for a sabbatical stay. J. X. M. is supported by Harvard University. N. G. is funded by the NSERC, the Canada Research Chairs Program, the Canadian Foundation for Innovation, and McGill University.

References

Aster, R. C., Thurber, C. H., & Borchers, B. (2005). *Parameter Estimation and Inverse Problems*. Amsterdam, Boston: Elsevier Academic Press.
Bouley, S., Baratoux, D., Matsuyama, I., Forget, F., Séjourné, A., Turbet, M., & Costard, F. (2016). Late Tharsis formation and implications for early Mars. *Nature*, *531*(7), 344–347.

Carr, M. H. (1995). The Martian drainage system and the origin of valley networks and fretted channels. *Journal of Geophysical Research*, *100*(E4), 7479–7507.
Chernick, M. R., González-Manteiga, W., Crujeiras, R. M., & Barrios, E. B. (2011). Bootstrap methods. In M. Lovric (Ed.), *International Encyclopedia of Statistical Science* (pp. 169–174). Berlin: Springer.
Citron, R. I., Manga, M., & Hemingway, D. J. (2018). Timing of oceans on Mars from shoreline deformation. *Nature*, *555*(7698), 643–646.
Clifford, S. M., & Parker, T. J. (2001). The evolution of the Martian hydrosphere: Implications for the fate of a primordial ocean and the current state of the northern plains. *Icarus*, *154*(1), 40–79.
Dahlen, F. A. (1976). The passive influence of the oceans upon the rotation of the Earth. *Geophysical Journal International*, *46*(2), 363–406.
Daradich, A., Mitrovica, J. X., Matsuyama, I., Perron, J. T., Manga, M., & Richards, M. A. (2008). Equilibrium rotational stability and figure of Mars. *Icarus*, *194*(2), 463–475.
di Achille, G., & Hynek, B. M. (2010). Ancient ocean on Mars supported by global distribution of deltas and valleys. *Nature Geoscience*, *3*(7), 459–463. https://doi.org/10.1038/ngeo891
DiBiase, R. A., Limaye, A. B., Scheingross, J. S., Fischer, W. W., & Lamb, M. P. (2013). Deltaic deposits at Aeolis Dorsa: Sedimentary evidence for a standing body of water on the northern plains of Mars. *Journal of Geophysical Research: Planets*, *118*, 1285–1302. https://doi.org/10.1002/jgre.20100
Efron, B. (1979). Bootstrap methods: Another look at the jackknife. *The Annals of Statistics*, *7*(1), 1–26.
Erkeling, G., Reiss, D., Hiesinger, H., Poulet, F., Carter, J., Ivanov, M. A., et al. (2012). Valleys, paleolakes and possible shorelines at the Libya Montes/Isidis boundary: Implications for the hydrologic evolution of Mars. *Icarus*, *219*(1), 393–413.
Evans, A. J., Andrews-Hanna, J. C., & Zuber, M. T. (2010). Geophysical limitations on the erosion history within Arabia Terra. *Journal of Geophysical Research*, *115*, E05007. https://doi.org/10.1029/2009JE003469
Fairén, A. G. (2010). A cold and wet Mars. *Icarus*, *208*(1), 165–175.
Fassett, C. I., & Head, J. W. III (2008). Valley network-fed, open-basin lakes on Mars: Distribution and implications for Noachian surface and subsurface hydrology. *Icarus*, *198*(1), 37–56.
Ghatan, G. J., & Zimbelman, J. R. (2006). Paucity of candidate coastal constructional landforms along proposed shorelines on Mars: Implications for a northern lowlands-filling ocean. *Icarus*, *185*(1), 171–196.
Gold, T. (1955). Instability of the Earth's axis of rotation. *Nature*, *175*, 526–529.
Goldreich, P., & Toomre, A. (1969). Some remarks on polar wandering. *Journal of Geophysical Research*, *74*(10), 2555–2567.
Grott, M., Baratoux, D., Hauber, E., Sautter, V., Mustard, J., Gasnault, O., et al. (2013). Long-term evolution of the Martian crust-mantle system. *Space Science Reviews*, *174*(1), 49–111.
Howard, A. D., Moore, J. M., & Irwin, R. P. (2005). An intense terminal epoch of widespread fluvial activity on early Mars: 1. Valley network incision and associated deposits. *Journal of Geophysical Research*, *110*, E12S14. https://doi.org/10.1029/2005JE002459
Hynek, B. M., Beach, M., & Hoke, M. R. T. (2010). Updated global map of Martian valley networks and implications for climate and hydrologic processes. *Journal of Geophysical Research*, *115*, E09008. https://doi.org/10.1029/2009JE003548
Hynek, B. M., & Phillips, R. J. (2003). New data reveal mature, integrated drainage systems on Mars indicative of past precipitation. *Geology*, *31*(9), 757–760.
Irwin, R. P., Craddock, R. A., & Howard, A. D. (2005). Interior channels in Martian valley networks: Discharge and runoff production. *Geology*, *33*(6), 489–492.
Irwin, R. P., Craddock, R. A., Howard, A. D., & Flemming, H. L. (2011). Topographic influences on development of Martian valley networks. *Journal of Geophysical Research*, *116*, E02005. https://doi.org/10.1029/2010JE003620
Irwin, R. P., Howard, A. D., & Craddock, R. A. (2008). Fluvial valley networks on Mars, *River Confluences, Tributaries and the Fluvial Network* (pp. 419–451). Chichester, UK: John Wiley.
Lambeck, K. (1980). *The Earth's Variable Rotation: Geophysical Causes and Consequences*. London: Cambridge University Press.
Leverington, D. W. (2011). A volcanic origin for the outflow channels of Mars: Key evidence and major implications. *Geomorphology*, *132*(3-4), 51–75.
Lewis, K. W., Aharonson, O., Grotzinger, J. P., Kirk, R. L., McEwen, A. S., & Suer, T.-A. (2008). Quasi-periodic bedding in the sedimentary rock record of Mars. *Science*, *322*(5907), 1532–1535.
Malin, M. C., & Edgett, K. S. (2000). Sedimentary rocks of early Mars. *Science*, *290*(5498), 1927–1937.
Matsubara, Y., Howard, A. D., & Gochenour, J. P. (2013). Hydrology of early Mars: Valley network incision. *Journal of Geophysical Research: Planets*, *118*, 1365–1387. https://doi.org/10.1002/jgre.20081
Matsuyama, I., & Manga, M. (2010). Mars without the equilibrium rotational figure, Tharsis, and the remnant rotational figure. *Journal of Geophysical Research*, *115*, E12020. https://doi.org/10.1029/2010JE003686
Michalski, J. R., & Bleacher, J. E. (2013). Supervolcanoes within an ancient volcanic province in Arabia Terra, Mars. *Nature*, *502*(7469), 47–52.
Moscardelli, L. (2014). Boulders of the Vastitas Borealis Formation: Potential origin and implications for an ancient Martian ocean. *GSA Today*, *24*, 4–10.
Mound, J. E., & Mitrovica, J. X. (1998). True polar wander as a mechanism for second-order sea-level variations. *Science*, *279*(5350), 534–537.
Mutch, T. A., & Saunders, R. S. (1976). The geologic development of Mars: A review. *Space Science Reviews*, *19*, 3–57.
Parker, T. J., Gorsline, D. S., Saunders, R. S., Pieri, D. C., & Schneeberger, D. M. (1993). Coastal geomorphology of the Martian northern plains. *Journal of Geophysical Research*, *98*(E6), 11,061–11,078.
Parker, T. J., Saunders, R. S., & Schneeberger, D. M. (1989). Transitional morphology in west Deuteronilus Mensae, Mars—Implications for modification of the lowland/upland boundary. *Icarus*, *82*, 111–145.
Perron, J. T., Mitrovica, J. X., Manga, M., Matsuyama, I., & Richards, M. A. (2007). Evidence for an ancient Martian ocean in the topography of deformed shorelines. *Nature*, *447*(7), 840–843. https://doi.org/10.1038/nature05873
Phillips, R. J., Zuber, M. T., Smrekar, S. E., Mellon, M. T., Head, J. W., Tanaka, K. L., et al. (2008). Mars north polar deposits: Stratigraphy, age, and geodynamical response. *Science*, *320*(5880), 1182–1185.
Phillips, R. J., Zuber, M. T., Solomon, S. C., Golombek, M. P., Jakosky, B. M., Banerdt, W. B., et al. (2001). Ancient geodynamics and global-scale hydrology on Mars. *Science*, *291*(5513), 2587–2591.
Smith, D. E., Zuber, M. T., Neumann, G. A., Guinness, E. A., & Slavney, S. (2003). Mars Global Surveyor Laser Altimeter Mission Experiment Gridded Data Record, MGS-M-MOLA-5-MEGDR-L3-V1.0, NASA Planetary Data System.
Tanaka, K. L., Skinner, J. A. Jr., Dohm, J. M., Irwin, R. P. III, Kolb, E. J., Fortezzo, C. M., et al. (2014). Geologic map of Mars: U.S. Geological Survey scientific investigations map 3292, scale 1:20,000,000, pamphlet 43 p. https://doi.org/10.3133/sim3292
Wordsworth, R. D. (2016). The climate of early Mars. *Annual Review of Earth and Planetary Sciences*, *44*(1), 381–408.

Wordsworth, R., Forget, F., Millour, E., Head, J. W., Madeleine, J. B., & Charnay, B. (2013). Global modelling of the early Martian climate under a denser CO_2 atmosphere: Water cycle and ice evolution. *Icarus*, *222*(1), 1–19.

Wordsworth, R. D., Kerber, L., Pierrehumbert, R. T., Forget, F., & Head, J. W. (2015). Comparison of "warm and wet" and "cold and icy" scenarios for early Mars in a 3-D climate model. *Journal of Geophysical Research: Planets*, *120*, 1201–1219. https://doi.org/10.1002/2015JE004787

Zharkov, V., & Gudkova, T. (2005). Construction of Martian interior model. *Solar System Research*, *39*(5), 343–373.

Zuber, M. T., & Smith, D. E. (1997). Mars without Tharsis. *Journal of Geophysical Research*, *102*(E12), 28,673–28,685.